Geophysical Research Letters

RESEARCH LETTER
10.1029/2019GL083339

A New Signal of the Solar Magnetic Cycle: Opposite Shifts of Weak Magnetic Field Distributions in the Two Hemispheres

Tibebu Getachew[1], **Ilpo Virtanen**[1], **and Kalevi Mursula**[1]

[1]ReSoLVE Centre of Excellence, Space Climate Research Unit, University of Oulu, Oulu, Finland

Key Points:
- Shifts of weak photospheric magnetic field distributions in the two hemispheres follow the evolution of the trailing flux
- The hemispheric shifts have always the same sign as the polarity of the polar field in the respective hemisphere and solar cycle
- Hemispheric shifts have opposite sign, but the Southern Hemisphere shifts are systematically larger than in the Northern Hemisphere

Correspondence to:
T. Getachew,
tibebu.ayalew@oulu.fi

Citation:
Getachew, T., Virtanen, I., & Mursula, K. (2019). A new signal of the solar magnetic cycle: Opposite shifts of weak magnetic field distributions in the two hemispheres. *Geophysical Research Letters*, *46*, 9327–9333. https://doi.org/10.1029/2019GL083339

Received 16 APR 2019
Accepted 24 JUL 2019
Accepted article online 30 JUL 2019
Published online 20 AUG 2019

Abstract We study the asymmetric distribution of weak photospheric magnetic field values in the two hemispheres separately using synoptic maps from Solar Dynamics Observatory/Helioseismic and Magnetic Imager, Synoptic Optical Long-term Investigations of the Sun/Vector SpectroMagnetograph, and Wilcox Solar Observatory during Solar Cycles 21–24. We calculate the weak-field asymmetry (shift) by fitting the distributions of weak-field values to a shifted Gaussian. Hemispheric shifts derived from the three data sets agree very well and increase systematically when reducing the spatial resolution of the map. Shifts of the Northern and Southern Hemispheres are typically opposite to each other. Shifts follow the evolution of the trailing flux and have a strong solar cycle variation with maxima in the early to mid declining phase of the solar cycle. The sign of the hemispheric weak-field shift is always the same as the polarity of the polar field in the respective hemisphere and solar cycle. We also find that shifts in the south are systematically larger in absolute value than in the north.

1. Introduction

Sunspot cycle is a manifestation of the waxing and waning of intense magnetic field regions like sunspots on the solar surface. Since the magnetic polarity changes every 11 years (Hale et al., 1919), the solar magnetic cycle (the Hale cycle) is 22 years, consisting of two sunspot cycles (for a historical review, see, e.g., Stenflo, 2015; van Driel-Gesztelyi & Green, 2015). While sunspot magnetic fields have been measured since the early twentieth century (Hale et al., 1919), the magnetic field of the whole photosphere has been measured only since 1950s (Babcock, 1953), with one of the longest consecutive series of measurements made at the Wilcox Solar Observatory (WSO) since 1970s (Hoeksema, 1984, 2010; Svalgaard et al., 1978).

Sunspots emerge at low to mid latitudes of the solar surface, producing tilted bipolar magnetic regions (BMRs). The large-scale magnetic field observed at the solar photospheric surface is mainly formed by the evolution (diffusion, transport, etc.) of BMRs. According to Joy's law, the axis of the bipolar regions is tilted with respect to the east-west direction, the leading polarity being at a slightly lower latitude than the trailing one. The trailing polarity flux of the decaying BMRs forms poleward directed surges, which cancel the old polar field and, eventually, create the new field of opposite polarity (Babcock, 1961; Leighton, 1969). Because the magnetic polarity of BMRs is opposite in the two hemispheres, the polar fields are also opposite to each other during most of the solar cycle. However, the evolution of surges is not identical in the two hemispheres. Moreover, the leading flux may also cause surges (so called countersurges, Ulrich & Tran, 2013), which also affect the large-scale field at mid and high latitudes.

The measured photospheric magnetic field consists mainly of rather weak fields than strong field values, irrespective of measurement accuracy. However, a small number of strong field values carry most of the total magnetic flux (Stenflo, 1982). Due to improved observational and diagnostic capabilities, there has been an increasing interest in the study of weak photospheric magnetic field values (e.g., Lites, 2002; Berger & Lites, 2002, 2003; Stenflo, 2010, 2014). We have recently shown (Getachew et al., 2019) that the distribution of weak-field values of the photospheric magnetic field is often asymmetric so that the distribution is slightly shifted toward either polarity. This shift was seen to be systematic in several simultaneous data sets. We argued that these weak-field shifts reflect a real asymmetry in the distribution of positive and negative weak-field values produced most effectively at the spatial scale of supergranulation (Getachew et al., 2019).

In this paper we study the distribution of weak-field values and the related weak-field asymmetry (shift) separately for the Northern and Southern Hemispheres using high-resolution data from the Helioseismic and Magnetic Imager (HMI) on board the Solar Dynamics Observatory and from the Synoptic Optical Long-term Investigations of the Sun (SOLIS) Vector SpectroMagnetograph (VSM), as well as low-resolution data from the WSO. The paper is organized as follows. Section 2 presents the data and methods used in this study. Section 3 studies on the hemispheric weak-field shifts in HMI data, and section 4 the same for SOLIS/VSM data. Section 5 presents the long-term evolution of hemispheric shifts using WSO data. Finally, we discuss the results and give our conclusions in section 6.

2. Data and Methods

In this paper we use synoptic maps of the photospheric pseudoradial (line of sight divided by cosine of latitude) magnetic field measured at HMI, SOLIS/VSM, and WSO to calculate the hemispheric weak-field asymmetry. HMI synoptic maps of the pseudoradial field have a resolution of 3,600 * 1,440 pixels equally spaced in longitude and sine latitude (Hayashi et al., 2015; Hoeksema et al., 2014; Liu et al., 2012). We note that the possible random zero offsets of the high-resolution HMI magnetograms are removed when constructing these maps (see Liu et al., 2012). The HMI synoptic maps included in this paper cover Carrington rotations (CRs) 2,097–2,214, that is, the time interval from 2010.4–2019.1. We derived four additional sets of medium- and low-resolution HMI synoptic maps (360 * 180, 180 * 72, 120 * 48, and 72 * 30) from the 3,600 * 1,440 synoptic maps using simple block averaging method (see Getachew et al., 2019) in order to investigate the effect of data resolution on the hemispheric weak-field asymmetries.

High-resolution synoptic maps of the (pseudoradial) photospheric magnetic field have been produced at the National Solar Observatory (NSO) using SOLIS/VSM instrument for CR 2007–2196, that is, between 2003.7–2017.8. The SOLIS/VSM synoptic maps used in this study have 1,800 * 900 pixels equally spaced in longitude and sine latitude, from which we calculated four sets of lower-resolution synoptic maps (360 * 180, 180 * 75, 120 * 50, and 72 * 30). VSM synoptic maps give the pseudoradial fields without polar filling. (Details on SOLIS/VSM data can be found, e.g., in Bertello et al., 2014).

The WSO synoptic maps (of the line-of-sight field) have a rather poor resolution of only 72 * 30 pixels in longitude and sine latitude (Hoeksema, 1984). We calculated the pseudoradial field from the line-of-sight magnetic fields. In this study we used all the 569 published F-data (where missing data are filled by interpolation) WSO synoptic maps from CR 1642–2210, that is, between 1976.3 and 2018.8. Note that in 1996–1999 and in 2001.1–2001.5 the WSO data are erroneous and in clear disagreement with other data (see, e.g., Virtanen & Mursula, 2016, 2017). This period of erroneous data is left out from the analysis of this paper. The WSO measurements are good in that the same instrumentation has been in operation since measurements have started. (Details about the WSO magnetograph, data calibration and reduction methods can be found, e.g., in Hoeksema, 1984).

We calculate the weak-field shifts in the same way as in Getachew et al. (2019). The histogram distribution of weak-field values (here within $\pm 10G$; note that results are insensitive to the range, as discussed by Getachew et al., 2019) for each synoptic map, separately for Northern and Southern Hemispheres, is fitted with a shifted Gaussian:

$$\phi = c \exp\left(-\frac{1}{2}\left(\frac{B_i - a}{b}\right)^2\right), \tag{1}$$

where B_i are the observed (weak) field values and the three fit parameters a, b, and c give the position of the peak (the weak-field shift), the width of the Gaussian distribution (standard deviation), and the amplitude, respectively.

3. Hemispheric Weak-Field Shifts of HMI

Figure 1 shows the HMI weak-field shift values for each synoptic map at the five resolutions mentioned above. The top panel presents the shift values using the full synoptic maps (cf. Figure 3 in Getachew et al., 2019), and the middle and bottom panels show the shifts using only the Northern and Southern Hemispheres of the synoptic map, respectively. The top panel shows that the full-map shifts mainly occur at the same time and have the same sign (positive or negative) for all five resolutions. The same is true for the hemispheric

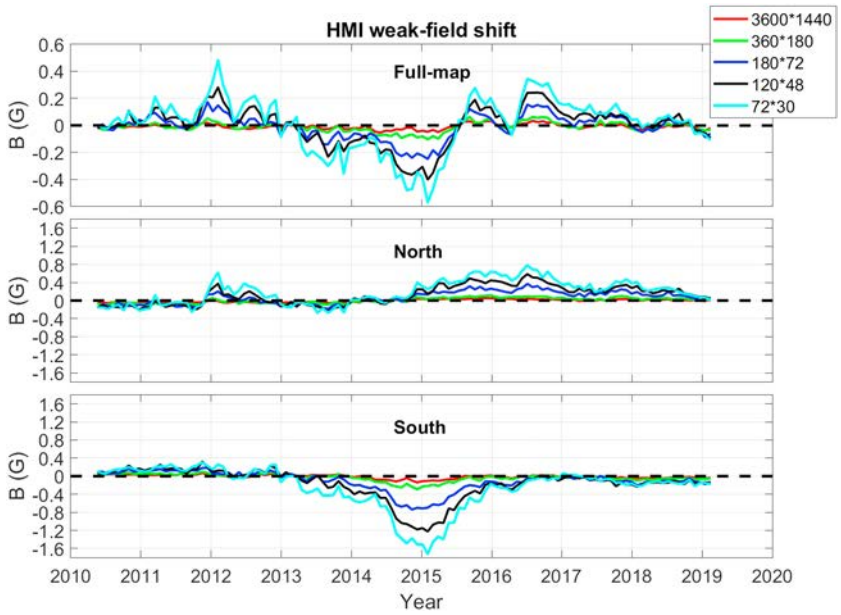

Figure 1. Weak-field shifts of HMI synoptic maps of 3,600 * 1,440 (red line), 360 * 180 (green line), 180 * 72 (blue line), 120 * 48 (black line), and 72 * 30 (cyan line) resolution. The top panel uses data from full synoptic maps, while the middle and bottom panels use data only from the Northern and Southern Hemispheres, respectively.
HMI = Helioseismic and Magnetic Imager.

weak-field shifts in the two other panels of Figure 1. Also, for all three cases (full-map, Northern and Southern Hemispheres) the weak-field shifts increase with decreasing resolution of the maps, as already found for full maps in Getachew et al. (2019). Shifts increase significantly when the resolution decreases from 360 * 180 to 180 * 72, reflecting the approach to the supergranulation scale of the photospheric field (Getachew et al., 2019). Note that the full-map shifts are typically quite close to the sum of the northern and southern shifts of the respective rotation. However, this is not always exactly the case, because the hemispheric distributions may be occasionally quite different.

Figure 1 (middle panel) shows that the Northern Hemisphere has a weak negative shift in 2010–2011, a clearly larger, positive shift in 2012 and then again a weak, mainly negative shift in 2013. Since 2014, until the end of data in 2019, the Northern Hemisphere has a fairly large, systematically positive weak-field shift.

The Southern Hemisphere (Figure 1, bottom panel) has a rather weak, mostly positive shift in 2010–2012. From 2013 onward, the southern shift is mostly negative and attains very large values in 2014–2015. Accordingly, the shifts in the Northern and Southern Hemispheres were oppositely directed for most of the HMI period. Out of 118 rotations included in Figure 1, the Northern and Southern Hemispheres have oppositely

Table 1
Mean Values of HMI Hemispheric Weak-Field Shifts (in Gauss) Using All Shifts and Dominantly Signed Shifts in Each Hemisphere

Hemisphere	Mean value of	3,600 * 1,440	360 * 180	180 * 72	120 * 48	72 * 30
Northern	all shifts	−0.007	0.004	0.066	0.122	0.184
		(−0.013, −0.0004)	(−0.007, 0.015)	(0.041, 0.091)	(0.084, 0.160)	(0.136, 0.233)
	positive shifts	0.027	0.056	0.150	0.242	0.320
		(0.023, 0.031)	(0.049, 0.063)	(0.130, 0.169)	(0.210, 0.274)	(0.280, 0.363)
Southern	all shifts	−0.013	−0.032	−0.107	−0.171	−0.244
		(−0.021, −0.005)	(−0.047, −0.018)	(−0.147, −0.068)	(−0.234, −0.108)	(−0.330, −0.161)
	negative shifts	−0.042	−0.074	−0.204	−0.320	−0.420
		(−0.050, −0.034)	(−0.090, −0.058)	(−0.249, −0.159)	(−0.395, −0.244)	(−0.514, −0.317)

*Note.*The upper and lower confidence intervals are given in parentheses. HMI = Helioseismic and Magnetic Imager.

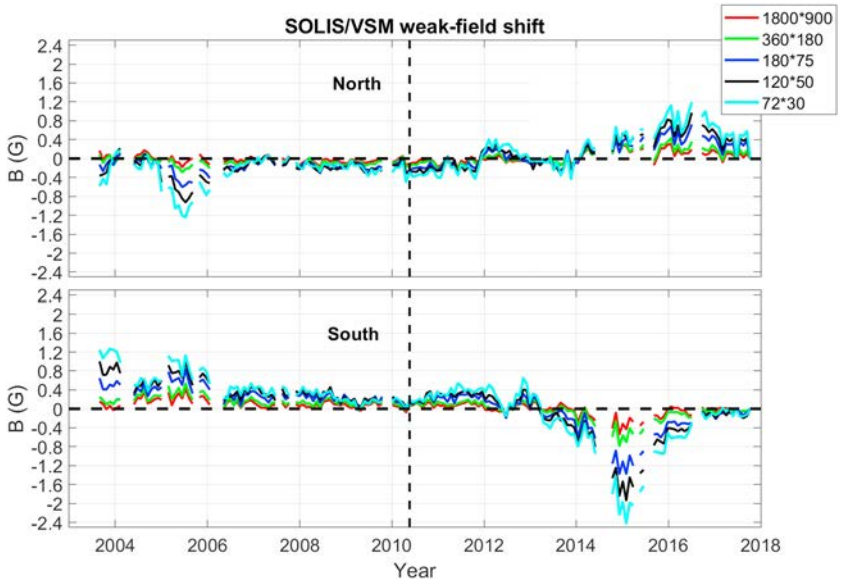

Figure 2. Hemispheric weak-field shifts of SOLIS/VSM synoptic map for 1,800 * 900 (red line), 360 * 180 (green line), 180 * 75 (blue line), 120 * 50 (black line), and 72 * 30 (cyan line) resolutions. The upper panel is for the Northern Hemisphere, and lower panel is for the Southern Hemisphere. The start time of Helioseismic and Magnetic Imager data is marked by dashed vertical line. SOLIS = Synoptic Optical Long-term Investigations of the Sun; VSM = Vector SpectroMagnetograph.

oriented shifts at least in 87 rotations (74%). Thus, there is a clear tendency for the simultaneous shifts to be oppositely oriented in the Northern and Southern Hemispheres.

Table 1 gives the mean values of HMI hemispheric shifts with lower and upper limits at 95% given in parenthesis. In order to calculate the lower and upper confidence intervals (CI) of the mean values of shifts, we applied the Student's t test given as

$$CI = \frac{1}{n}\sum_{i=1}^{n}\mu_i \pm S_\mu t_{\alpha,n-1} \tag{2}$$

where S_μ is the error of the mean of individual shifts μ_i, and $t_{\alpha,n-1}$ is the precalculated statistic value for the t distribution, where α is the significance level (for a 95% confidence interval, $\alpha = 0.025$) and n is the number of shift values ($n = 118$ for all shifts of HMI data).

We have calculated the means of all shifts over the full time interval and also the means of the dominantly signed shifts in either hemispheres, that is, positive in the north and negative in the south. Table 1 shows that the positive shifts in the north and the negative shifts in the south increase (in absolute value) systematically with reducing spatial resolution, from about 0.03 (−0.04) in the 3,600 * 1,440 maps to 0.32 (−0.42) in the 72 * 30 maps in the north (south, respectively). The largest step in this decadal increase occurs between 360 * 180 and 180 * 72, where shift increases roughly by a factor of 2.5 to 3. Note also that the negative shifts in the south are systematically (for all resolutions) larger in absolute value than the positive shifts in the north.

4. Hemispheric Weak-Field Shifts of SOLIS/VSM

Figure 2 shows the hemispheric weak-field shifts for SOLIS/VSM synoptic maps at the five resolutions of 1,800 * 900, 360 * 180, 180 * 75, 120 * 50, and 72 * 30 in 2003.7–2017.8. Comparing Figures 1 and 2, in most of the simultaneous rotations, the sign of both the Northern and Southern Hemisphere shifts is the same in HMI and SOLIS/VSM. Out of the 100 rotations of the overlapping time, 74 (87) HMI shifts of 360 * 180 (72 * 30 maps, respectively) maps have the same sign as SOLIS/VSM maps in the Northern Hemisphere, and 77 (82) shifts in the Southern Hemisphere. This gives strong evidence for the validity and universality of the obtained hemispheric shifts.

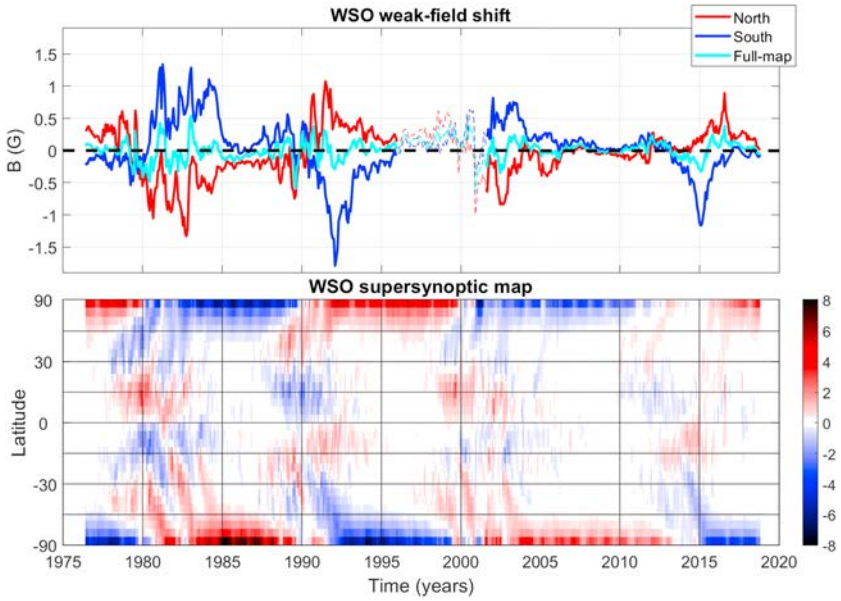

Figure 3. The top panel shows WSO synoptic map weak-field shifts separately for the Northern Hemisphere (red line), Southern Hemisphere (blue line), and the full-disk maps (cyan line). Weak-field asymmetries during the erroneous data period (1996–2001) are shown by a dashed line. The bottom panel shows photospheric magnetic field butterfly diagram (supersynoptic map) from WSO synoptic maps. In the bottom panel plot, red color indicates positive (outward) polarity and blue negative (inward) polarity. Units are in gauss.

We have also calculated the correlation coefficients (r) and the corresponding p values between SOLIS/VSM and HMI shifts in the Northern and Southern Hemispheres for all possible resolution combinations (5 SOLIS/VSM × 5 HMI). For all 25 combinations and for both hemispheres, the correlations are high and extremely significant. Correlations were overall slightly more important in the south than in the north. The lowest correlation was found in the Northern Hemisphere between the highest SOLIS/VSM and lowest HMI resolution ($r = 0.6$, $p < 10^{-9}$) and the highest correlation in the Southern Hemisphere for the lowest resolution of both data sets ($r = 0.96$, $p < 10^{-51}$).

Figure 2 shows that the SOLIS/VSM shifts are mostly negative in the Northern Hemisphere in 2003–2011 and mostly positive thereafter (cf. Figure 1). The largest negative shifts in the north are found in 2005. SOLIS/VSM shifts in the Southern Hemisphere are mostly positive in 2003–2012 and mostly negative thereafter. The highest positive shifts in the south are found in 2004–2005. These results further strengthen the overall anticorrelation between the northern and southern shifts, as indicated earlier by HMI results. They also suggest that there is a change in the sign of the hemispheric shifts from one solar cycle to the next.

The mean SOLIS/VSM shifts are systematically larger than the HMI shifts for the same resolution and hemisphere (note the different scales of y axis in Figures 1 and 2). The SOLIS/HMI ratios vary from a factor of about 2 for 360 * 180 resolution to only about 30–50% for 72 * 30 resolution. The hemispheric shifts of SOLIS/VSM increase systematically when the resolution decreases, as already seen for HMI. Also similarly with HMI, the SOLIS/VSM mean shifts are larger in the south than in the north.

5. Hemispheric Weak-Field Shifts of WSO

The top panel of Figure 3 shows the full-map and hemispheric weak-field shifts for WSO in CR 1,642–2,210, that is, between 1976.3 and 2018.8, including four solar cycles. Figure 3 (top panel) verifies that the northern and southern shifts evolve roughly in anticorrelation and depict a clear variation over the solar cycle. Hemispheric shifts have maxima in the early to mid declining phase of the solar cycle and decrease to very small absolute values until the solar minimum but change their sign typically only in the late ascending to maximum phase of the solar cycle.

The bottom panel of Figure 3 shows the map of longitudinally averaged magnetic field derived from WSO synoptic maps, the so-called photospheric supersynoptic map, also called the magnetic field butterfly

Table 2
Mean Values of WSO Hemispheric Weak-Field Shifts in Gauss for Each Solar Cycle

Hemisphere		SC21	SC22	SC23	SC24
Northern	time	1979.6–1990.3	1990.3–1996	2001–2011.9	2011.9–2018.8
	all shifts	−0.388 (−0.437, −0.339)	0.367 (0.313, 0.421)	−0.147 (−0.182, −0.112)	0.196 (0.161, 0.230)
	dominant shift	−0.403 (−0.451, −0.356)	0.367 (0.313, 0.421)	−0.193 (−0.233, −0.154)	0.213 (0.179, 0.248)
Southern	time	1980.4–1990.4	1990.4–1996	2001–2013.2	2013.9–2018.8
	all shifts	0.396 (0.334, 0.459)	−0.516 (−0.612, −0.419)	0.196 (0.166, 0.227)	−0.272 (−0.343, −0.201)
	dominant shift	0.444 (0.382, 0.506)	−0.523 (−0.620, −0.426)	0.202 (0.171, 0.233)	−0.314 (−0.388, −0.239)

Note. The upper and lower confidence intervals are given in parentheses. WSO = Wilcox Solar Observatory.

diagram. This diagram depicts the overall pattern of the solar magnetic cycle, that is, the alteration of magnetic polarity according to the 22-year cycle at the solar surface. It also shows the transport of surges of new flux to the poles and the eventual reversal of the polar fields.

Figure 3 suggests that hemispheric weak-field shifts are related to the poleward surges of magnetic flux and the evolution of polar fields. The different timing of surges in the north and south (see, e.g., 1990 and 1991) is also seen in the different time evolution of the Northern and Southern Hemisphere weak-field shifts.

Table 2 presents the mean shift for each hemisphere and each solar cycle, separately. The times were determined from the change of the sign of the shift in the corresponding hemisphere. Table 2 shows clearly that the mean shifts follow the sign (polarity) of the solar pole in that hemisphere and cycle. Moreover, in each cycle (and overall) the Southern Hemisphere shifts are somewhat larger than in the Northern Hemisphere. This difference is particularly strong during the two even cycles where the shift ratios are about 1.42 and 1.47 for Solar Cycle 22 and Solar Cycle 24, while they are only about 1.1 and 1.05 for the two odd cycles.

The WSO hemispheric shifts agree very well with the signs of the corresponding SOLIS/VSM and HMI shifts, and the absolute values of the WSO shifts are typically between those of HMI and SOLIS/VSM. Out of the 169 overlapping rotations, 117, 126, 133, 139, and 140 SOLIS/VSM (1,800 * 900, 360 * 180, 180 * 75, 120 * 50, and 72 * 30) shifts had the same sign in the north as WSO and 136, 151, 158, 157 and 157 shifts in the south. Correlation in hemispheric shifts between WSO and SOLIS/VSM are all high and statistically significant, at least with $r = 0.5$ ($p < 10^{-10}$). Correlations are slightly better for the south than north, as found earlier between SOLIS/VSM and HMI.

6. Discussion and Conclusions

In this paper we have studied the hemispheric shifts of weak photospheric magnetic field values using HMI, SOLIS/VSM and WSO data sets at different resolutions. Hemispheric shifts were calculated by fitting the histogram distribution of hemispheric weak-field values (here within $\pm 10G$) for each synoptic map to a shifted Gaussian (Getachew et al., 2019).

As found earlier for the full-map shifts (Getachew et al., 2019), the hemispheric shifts have systematically the same sign for different map resolutions and increase with reduced spatial resolution. The shifts increase significantly in both hemispheres when the resolution decreases from 360 * 180 to 180 * 72, reflecting the approach to the supergranulation scale of the photospheric field (Getachew et al., 2019). Moreover, the shifts have mainly the same sign for simultaneous rotations for all the three independent instruments (HMI, SOLIS/VSM, and WSO) in each hemisphere. The absolute values of the shifts are somewhat different, with SOLIS/VSM shifts being largest and HMI smallest, but this difference decreases when reducing the map resolution.

We find that the Northern and Southern Hemisphere shifts are typically opposite to each other, but the simultaneous shifts do not often have the same (absolute) magnitude. These differences in the magnitudes and time evolutions of the hemispheric shifts explain the full-map shifts studied earlier in Getachew et al. (2019).

Hemispheric shifts depict a clear evolution over the solar cycle. They change their sign in the late ascending or maximum phase of the cycle and attain their maximum in the early to mid declining phase. The hemispheric shifts have always the same sign as the polarity of the respective pole of the future solar minimum. Thus, the hemispheric shifts have a relation to the evolution of the polar fields.

We found that the Southern Hemisphere shifts are systematically larger than in the north in all the three data sets and solar cycles. This is particularly true for the even solar cycles (SC22 and SC24), where the southern shifts are roughly 50% larger at WSO resolution than the northern shifts. This difference may contribute to the earlier observed stronger field intensity in the south and the related southward shift of the heliospheric current sheet, also called the bashful ballerina phenomenon (Hiltula & Mursula, 2006; Mursula & Hiltula, 2003, 2004; Virtanen & Mursula, 2010; 2014, 2016; Zhao et al., 2005).

Acknowledgments
We acknowledge the financial support by the Academy of Finland to the ReSoLVE Centre of Excellence (Project 307411). Wilcox Solar Observatory data used in this study were obtained via the web site http://wso.stanford.edu courtesy of J. T. Hoeksema. Data were acquired by SOLIS instruments operated by NISP/NSO/AURA/NSF. HMI data are courtesy of the Joint Science Operations Center (JSOC) Science Data Processing team at Stanford University. Data used in this study were obtained from the following web sites: WSO (http://wso.stanford.edu), SOLIS (http://solis.nso.edu/0/vsm/vsm&urluscore;maps.php), and HMI (http://jsoc.stanford.edu/data/hmi/synoptic).

References

Babcock, H. W. (1953). The solar magnetograph. *The Astrophysical Journal*, *118*, 387. https://doi.org/10.1086/145767
Babcock, H. W. (1961). The topology of the Sun's magnetic field and the 22-year cycle. *The Astrophysical Journal*, *133*, 572. https://doi.org/10.1086/147060
Berger, T. E., & Lites, B. W. (2002). Weak-field magnetogram calibration using advanced stokes polarimeter flux-density maps—I. Solar optical universal polarimeter calibration. *Solar Physics*, *208*(2), 181–210.
Berger, T. E., & Lites, B. W. (2003). Weak-field magnetogram calibration using advanced stokes polarimeter flux density maps—II. SOHO/MDI full-disk mode calibration. *Solar Physics*, *213*(2), 213–229. https://doi.org/10.1023/A:1023953716633
Bertello, L., Pevtsov, A. A., Petrie, G. J. D., & Keys, D. (2014). Uncertainties in solar synoptic magnetic flux maps. *Solar Physics*, *289*(7), 2419–2431.
Getachew, T., Virtanen, I., & Mursula, K. (2019). Asymmetric distribution of weak photospheric magnetic field values. *The Astrophysical Journal*, *874*(2), 116. https://doi.org/10.38471538-4357/ab0749
Hale, G. E., Ellerman, F., Nicholson, S. B., & Joy, A. H. (1919). The magnetic polarity of Sun-spots. *The Astrophysical Journal*, *49*, 153. https://doi.org/10.1086/142452
Hayashi, K., Hoeksema, J. T., Liu, Y., Bobra, M. G., Sun, X. D., & Norton, A. A. (2015). The Helioseismic and Magnetic Imager (HMI) vector magnetic field pipeline: Magnetohydrodynamics simulation module for the global solar corona. *Solar Physics*, *290*(5), 1507–1529.
Hiltula, T., & Mursula, K. (2006). Long dance of the bashful ballerina. *Geophysical Research Letters*, *33*, L03105. https://doi.org/10.1029/2005GL025198
Hoeksema, J. T. (1984). Structure and evolution of the large scale solar and heliospheric magnetic fields (Ph.D. Thesis), Stanford University, CA.
Hoeksema, J. T. (2010). Evolution of the large-scale magnetic field over three solar cycles. In Proceedings, IAU Symposium 264: Solar and stellar variability: Impact on earth and planets (pp. 222–228). Rio de Janeiro, Brazil. https://doi.org/10.1017/S1743921309992675
Hoeksema, J. T., Liu, Y., Hayashi, K., Sun, X., Schou, J., Couvidat, S., et al. (2014). The Helioseismic and Magnetic Imager (HMI) vector magnetic field pipeline: Overview and performance. *Solar Physics*, *289*(9), 3483–3530.
Leighton, R. B. (1969). A magneto-kinematic model of the solar cycle. *The Astrophysical Journal*, *156*, 1. https://doi.org/10.1086/149943
Lites, B. W. (2002). Characterization of magnetic flux in the quiet Sun. *The Astrophysical Journal*, *573*, 431–444. https://doi.org/10.1086/340120
Liu, Y., Hoeksema, J. T., Scherrer, P. H., Schou, J., Couvidat, S., Bush, R. I., et al. (2012). Comparison of line-of-sight magnetograms taken by the Solar Dynamics Observatory/Helioseismic and Magnetic Imager and Solar and Heliospheric Observatory/Michelson Doppler Imager. *Solar Physics*, *279*, 295–316. https://doi.org/10.1007/s11207-012-9976-x
Mursula, K., & Hiltula, T. (2003). Bashful ballerina: Southward shifted heliospheric current sheet. *Geophysical Research Letters*, *30*(22), 2135. https://doi.org/10.1029/2003GL018201
Mursula, K., & Hiltula, T. (2004). Systematically asymmetric heliospheric magnetic field: Evidence for a quadrupole mode and non-axisymmetry with polarity flip-flops. *Solar Physics*, *224*, 133–143. https://doi.org/10.1007/s11207-005-4977-7
Stenflo, J. O. (1982). The Hanle effect and the diagnostics of turbulent magnetic fields in the solar atmosphere. *Solar Physics*, *80*, 209–226. https://doi.org/10.1007/BF00147969
Stenflo, J. O. (2010). Distribution functions for magnetic fields on the quiet Sun. *Astronomy & Astrophysics*, *517*, A37. https://doi.org/10.1051/0004-6361/200913972
Stenflo, J. O. (2014). Nature of quiet-Sun magnetic fields.
Stenflo, J. O. (2015). History of solar magnetic fields since George Ellery Hale. *Space Science Reviews*, *210*, 5–35. https://doi.org/10.1007/s11214-015-0198-z
Svalgaard, L., Duvall Jr, T. L., & Scherrer, P. H. (1978). The strength of the Sun's polar fields. *Solar Physics*, *58*, 225–239. https://doi.org/10.1007/BF00157268
Ulrich, R. K., & Tran, T. (2013). The global solar magnetic field identification of traveling, long-lived ripples. *The Astrophysical Journal*, *768*(2), 189.
van Driel-Gesztelyi, L., & Green, L. M. (2015). Evolution of active regions. *Living Reviews in Solar Physics*, *12*, 1. https://doi.org/10.1007/lrsp-2015-1
Virtanen, I. I., & Mursula, K. (2010). Asymmetry of solar polar fields and the southward shift of HCS observed by Ulysses. *Journal of Geophysical Research*, *115*, A09110. https://doi.org/10.1029/2010JA015275
Virtanen, I. I., & Mursula, K. (2014). North-south asymmetric solar cycle evolution: Signatures in the photosphere and consequences in the corona. *The Astrophysical Journal*, *781*(2), 99.
Virtanen, I., & Mursula, K. (2016). Photospheric and coronal magnetic fields in six magnetographs. I. Consistent evolution of the bashful ballerina. *Astronomy & Astrophysics*, *591*, A78. https://doi.org/10.1051/0004-6361/201628096
Virtanen, I., & Mursula, K. (2017). Photospheric and coronal magnetic fields in six magnetographs. II. Harmonic scaling of field intensities. *Astronomy & Astrophysics*, *604*, A7. https://doi.org/10.1051/0004-6361/201730863
Zhao, X. P., Hoeksema, J. T., & Scherrer, P. H. (2005). Prediction and understanding of the north-south displacement of the heliospheric current sheet. *Journal of Geophysical Research*, *110*, A10101. https://doi.org/10.1029/2004JA010723